Near Surface Geophysics, 2009, 599-612

Fast, laterally smooth inversion of airborne time-domain electromagnetic data

Niels B. Christensen[1*], James E. Reid[2] and Max Halkjær[3]

[1] *Department of Earth Sciences, University of Aarhus, Hoegh Guldbergs Gade 2, 8000 Aarhus C, Denmark*
[2] *Geoforce Pty Ltd, 1/288 Victoria Rd, Malaga, 6090 Western Australia, Australia*
[3] *SkyTEM Aps, Tofteledet 18, 8330 Beder, Denmark*

Received November 2008, revision accepted August 2009

ABSTRACT

We present a fully developed, fast approximate method for 1D inversion of time-domain electromagnetic data. The method is applied to a helicopterborne transient electromagnetic data set from the Toolibin Lake area of Western Australia using the lateral parameter correlation method to ensure lateral smoothness of the inverted models.

The method is based on fast approximate forward computation of transient electromagnetic step responses and their derivatives with respect to the model parameters of a 1D model. The inversion is carried out with multi-layer models in an iterative, constrained least-squares inversion formulation including explicit formulation of the model regularization through a model covariance matrix. The method is 50 times faster than conventional inversion for a layered earth model and produces model sections of concatenated 1D models and contoured maps of mean conductivity in depth intervals almost indistinguishable from those of conventional inversion.

To ensure lateral smoothness of the model sections and to avoid spurious artefacts in the mean conductivity maps, the inversion is integrated with the lateral parameter correlation method. In this way, well determined parameters are allowed to influence the more poorly determined parameters in the survey area.

Applied to the Toolibin data set, the inversion produces model sections and conductivity maps that reveal the distribution of conductivity in the area and thereby the distribution of salinity. This information is crucial for any remediation effort aimed at alleviating the salinization problems.

INTRODUCTION

Transient electromagnetic (TEM) soundings have become one of the standard methods of environmental geophysics (Fittermann and Stewart 1986; Buselli *et al.* 1990; Hoekstra and Blohm 1990; Christensen and Sørensen 1998; Auken *et al.* 2006). TEM measurements delineate good conductors well, such as clay and salt water, thereby assisting hydrogeological modelling efforts by delivering information on important formation boundaries and formation characteristics.

Over the past two decades, airborne TEM methods have found widespread use in hydrogeophysical investigations, making it possible to cover large areas in a cost-effective way. Often huge data sets are collected with individual decay data stacked and binned along the flight lines. Data stacked for every 0.1 s at an acquisition speed of 25 m/s will give 400 soundings per kilometre, corresponding to a million soundings for a survey of 2,500 km. A recent review of helicopterborne time-domain electromagnetic systems can be found in Sattel (2006) and Spies and Woodgate (2005) presented recent results on salinity mapping with specific address to the Australian environment.

In the paper by Macnae (1997), a number of issues were identified as important targets for further research and among these were fast, trustworthy and easy-to-use tools for interpretation of both 1D and 3D targets. Fast methods for multidimensional inversion will not be discussed here but fast methods for 1D inversion have a fairly long history.

In the process of diffusion of TEM fields into the ground, the diffusion depth and diffusion velocity depend on the subsurface conductivity structure. A number of imaging methods are based on the variation of the diffusion velocity with conductivity (Nekut 1987; Macnae and Lamontagne 1987; Eaton and Hohmann 1989; Macnae *et al.* 1991). Essentially, these methods find the depth to an equivalent current filament as a function of time, from which the diffusion velocity and thereby the conductivity can be found. The conductivity is then ascribed to a depth equal to the image depth scaled with an ad hoc factor to produce the best results. The conductivity-depth imaging (CDI) of Stolz and Macnae (1997) is based on the step response and Stolz and

* nbc@geo.au.dk

Macnae (1998) presented a method for reducing arbitrary waveform transient EM data to the step response. The conductivity-depth images of Macnae *et al.* (1991) are available in the EMFlow software (Macnae *et al.* 1998) and they are an effective transformation of airborne electromagnetic (AEM) data provided the input data are well calibrated, broadband and low noise. Recently Sattel (2005) demonstrated the successful use of Zohdy's method in a fast inversion scheme.

Hydrogeophysical investigations require data to be of good enough quality to justify a quantitative inversion. Inversion with 2D and 3D models is not yet feasible because of the computational burden, so most often data are inverted using 1D models. With the speed of modern computers, inversion with 1D models no longer presents a problem, but inverting huge data sets can still be challenging in terms of computation time, especially because new interpretation techniques involve the simultaneous inversion of many soundings with lateral constraints between the 1D models (Auken and Christiansen 2004; Auken *et al.* 2005; Brodie and Sambridge 2006) to assure lateral continuity of the model sections of concatenated 1D models.

1D inversion is justified where lateral changes in conductivity are gradual. In this case, the pseudo-2D images produced by concatenating 1D models along the profile will give a good approximation to the real conductivity distribution. The effect of 3D structures on 1D interpretation of TEM data has been dealt with in a number of papers, e.g., Auken (1995), Hördt and Scholl (2004), Newman *et al.* (1987) and Goldman *et al.* (1994). In general, these studies show that if the geological environment consists of slowly varying 3D structures with moderate conductivity contrasts, the 1D inversion approach is viable. In environments with pronounced 3D model characteristics, 1D inversion is strongly influenced by 3D effects and will in many cases provide unreliable models with artefacts know as 'pantlegs'. However, though it is not sufficient to prove that 3D effects are not present, none of these typical model artefacts have been seen in the model sections of the inverted Toolibin data sets.

This paper has the dual aims of presenting an updated and mature version of the fast approximate inversion method of Christensen (2002) capable of modelling the complicated system response of a modern helicopterborne transient electromagnetic system and employing the method to invert the Toolibin Lake SkyTEM data set (Sørensen and Auken 2004) with application of the lateral parameter correlation method according to Christensen and Tølbøll (2009). In the following, the accuracy of the method in modelling the full system response will be documented and the inversion methodology will be presented. Regularization parameters for the vertical smoothness of the multi-layer inversion models and the lateral smoothness invoked by the lateral parameter correlation method (Christensen of Tølbøll 2008) will be pragmatically chosen based on a comparative study of the effect of different parameters. Then the helicopterborne system is introduced with specific regard to the Toolibin Lake survey together with a hydrological description of the area. The results of the interpretation are presented as model sections along the profile lines and as contoured maps of mean conductivity in elevation intervals and we shall compare the results of the fast approximate inversion with conventional inversion.

THE FAST APPROXIMATE INVERSION METHOD

Approximate forward mapping

The fast approximate inversion is based on a fast approximate forward mapping from conductivity as a function of depth to step response for a 1D layered model: $\sigma(z) \rightarrow B_L^{step}(t)$ (Christensen 2002). This forward mapping consists of two consecutive mappings: 1) a mapping from conductivity as a function of depth to apparent conductivity as a function of time: $\sigma(z) \rightarrow \sigma_a(t)$, followed by 2) a substitution of the apparent conductivity into a half-space response: $B_L^{step}(t) = B_{HSP}^{step}(t, \sigma_a(t))$. The step response for a layered model is by definition given as the half-space response at the same delay time for a half-space conductivity equal to the apparent conductivity. The first mapping, $\sigma(z) \rightarrow \sigma_a(t)$, is generic, i.e., it is the same for all transmitter-receiver (T_x–R_x) configurations and field components. In the second mapping, $B_L^{step}(t) = B_{HSP}^{step}(t, \sigma_a(t))$, the half-space response is specific for the configuration and field component in question. However, half-space responses need only be calculated once at program start. In the case of airborne systems, a half-space response must be calculated for a series of heights with a proper density to allow accurate interpolation.

The generic mapping is given by the integral equation

$$\sigma_a(t) = \int_0^\infty \sigma(z)\, w\left(z, t, \sigma_a(t)\right) dz \tag{1}$$

where w is a weight function that depends on the apparent conductivity. In this way the slower diffusion through good conductors and the faster diffusion through poor conductors are taken into account, i.e., the mapping is model adaptive.

For a layered earth model with N layers with conductivities $\sigma_1, \sigma_2 \ldots, \sigma_N$, and upper layer boundaries $z_1, z_2, \ldots, z_N$, $z_1 = 0$

$$\begin{aligned}\sigma_a(t) &= \sigma_1 \int_1^{z_2} w(z,t,\sigma_a(t))dz + \sigma_2 \int_2^{z_3} w(z,t,\sigma_a(t))dz + \\ &\qquad \cdots + \sigma_N \int_N^{\infty} w(z,t,\sigma_a(t))dz \\ &= \sigma_1\left[1 - W(z_2)\right] + \sigma_2\left[W(z_2) - W(z_3)\right] + \cdots + \sigma_N\left[W(z_N)\right]\end{aligned} \tag{2}$$

where $W(z, t, \sigma_a(t))$ is the integrated weight function

$$W(z,t,\sigma) = \int_z^\infty w(z',t,\sigma)dz' \tag{3}$$

The integrated weight function is chosen as

$$W(z,t,\sigma) = \operatorname{erfc}(\theta z) \;,\; \theta = \sqrt{\frac{\mu\sigma}{ct}} \tag{4}$$

and the weight function is consequently given by

$$w(z,t,\sigma) = \frac{2\theta}{\sqrt{\pi}} \exp\left(-\theta^2 z^2\right), \tag{5}$$

which is a different choice from the linear function used in

Christensen (2002). Many different weight functions will be equally good but the one defined above has continuous derivatives that makes it perform better in the convolutions necessary to model the system response. The parameter c scales the depth extent of the sensitivity function and eventually the depth scaling of the resulting models after inversion. It is chosen to minimize the difference between a series of test models and the approximate inversion results (Christensen 2002).

Substituting the apparent conductivity into the half-space step response, we have computed the layered step response $B_L^{step}(t) = B_{HSP}^{step}(t, \sigma_a(\sim t))$. However, the measured response in the time-domain is a convolution of the step response with operators accounting for repetition, a filter function defining the cutoff of the receiver coil, a filter function pertaining to the band limitation of the receiver amplifier, the second derivative of the transmitter waveform and the integration over the gate:

$$B_{meas} = B_L^{step}(t) * F_{rep}(t) * F_{Rx}(t) * F_{Amp}(t) * I''(t) * F_{gate}(t) \quad (6)$$

Looking at equation (2) is readily seen that the derivatives $\partial\sigma_a / \partial\sigma_i$ are given as

$$\frac{\partial\sigma_a}{\partial\sigma_i} = W(z_i) - W(z_{i+1}) \quad (7)$$

and the derivatives of the layered step response are then given by

$$\frac{\partial B_L^{step}(t)}{\partial\sigma_i} = \frac{\partial B_L^{step}(t)}{\partial\sigma_a} \cdot \frac{\partial\sigma_a}{\partial\sigma_i} \quad (8)$$

However, the layered step response is a function of (t/σ) and not of t and σ independently, so

$$\frac{\partial B_L^{step}(t)}{\partial\sigma_a} = \frac{t}{\sigma_a} \cdot \frac{\partial B_L^{step}(t)}{\partial t} \quad (9)$$

The derivatives of the measured response are then given by a similar convolution as in equation (6). Derivatives with respect to layer thicknesses can be expressed in terms of derivatives with respect to conductivity (Christensen 2002) but the fast approximate inversion is used only for multi-layer models for which only derivatives with respect to conductivity are relevant.

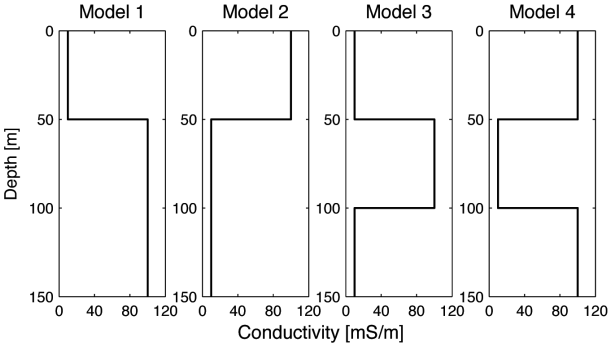

FIGURE 1
The conductivity as a function of depth for the four test models.

Figure 1 shows four models – two-layer models with a high or low conductivity half-space and three-layer models with a high or low conductivity second layer. In Fig. 2 the measured responses are shown for four models for conventional computations and for the fast approximate modelling. Conventional computation is carried out using the formulas in Ward and Hohman (1987) and the fast Hankel transform filters by Christensen (1990).

INVERSION METHODOLOGY

There are numerous approaches to the inversion of electromagnetic (EM) data with a 1D model consisting of horizontal, homogeneous and isotropic layers. The one used in this study is a well-established iterative damped least squares approach (Menke 1989). Formally, the model update at the n-th iteration is given by

$$\boldsymbol{m}_{n+1} = \boldsymbol{m}_n + \left[\boldsymbol{G}_n^T \boldsymbol{C}_{obs}^{-1} \boldsymbol{G}_n + \boldsymbol{C}_{prior}^{-1} + \boldsymbol{C}_m^{-1} + \lambda \boldsymbol{I}\right]^{-1} \cdot$$

$$\left[\boldsymbol{G}_n^T \boldsymbol{C}_{obs}^{-1} \left(\boldsymbol{d}_{obs} - \boldsymbol{g}(\boldsymbol{m}_n)\right) + \boldsymbol{C}_{prior}^{-1} \left(\boldsymbol{m}_{prior} - \boldsymbol{m}_n\right) + \boldsymbol{C}_m^{-1} \left(\boldsymbol{m}_{prior} - \boldsymbol{m}_n\right)\right] \quad (10)$$

where $\boldsymbol{m}$ is the model vector containing the logarithm of the model parameters, $\boldsymbol{G}$ is the Jacobian matrix containing the derivatives of the data with respect to the model parameters, T is the matrix transpose, $\boldsymbol{C}_{obs}$ is the data error covariance matrix, $\boldsymbol{C}_{prior}$ is the covariance matrix of the prior model, $\boldsymbol{C}_m$ is a model covariance matrix imposing the vertical smoothness constraint of the multi-layer models, λ is the Marquard damping factor, $\mathbf{I}$ is the identity matrix, $\boldsymbol{d}_{obs}$ is the field data vector, $\boldsymbol{g}(\boldsymbol{m}_n)$ is the non-linear forward response vector of the n-th model and $\boldsymbol{m}_{prior}$ is the prior model vector. In this study, as is most often the case, the data noise is assumed to be uncorrelated, implying that $\boldsymbol{C}_{obs}$ is a diagonal matrix.

The model parameter uncertainty estimate relies on a linear approximation to the posterior covariance matrix, $\boldsymbol{C}_{est}$, given by

$$C_{est} = \left[\mathbf{G}^T \mathbf{C}_{obs}^{-1} \mathbf{G} + \mathbf{C}_{prior}^{-1} + \mathbf{C}_m^{-1}\right]^{-1} \quad (11)$$

where $\boldsymbol{G}$ is based on the model achieved after the last iteration. The analysis is expressed through the standard deviations of the model parameters obtained as the square root of the diagonal elements of $\boldsymbol{C}_{est}$ (e.g., Inman *et al.* 1975).

The multi-layer model

The models used in the approximate inversion are multi-layer models, sometimes called 'smooth' models, where the subsurface is divided into a large number of layers. In the iterative inversion, the layer boundaries are kept fixed and only the layer conductivities are changed in the inversion. In this study we have used a 30-layer model where the depths to the layer boundaries increase downwards as a hyperbolic sine of the layer number. In this way, the depths to the layer boundaries increase linearly for small depths so that the top layers are all of approximately the same thickness and the depths to the layer boundaries increase exponentially at large depths so that the thickness of a layer is a

factor times the previous one.

In general, the thickness of the top layer and the depth to the lowest layer boundary are chosen according to the survey aims and the expected depth of investigation for a given system configuration. In this survey, our 30-layer model, the top layer is 2 m thick and the deepest layer boundary is at a depth of 270 m. The asymptotic exponential factor is 1.127, corresponding to about 19 layers per decade. The initial model is a homogeneous half-space with a conductivity of 33.33 mS/m.

A proper multi-layer model must be an oversampling of the subsurface in relation to the information contents of the data, i.e., none of the layers must be individually resolved and the depth to the bottom layer boundary must be well below the penetration depth of the data. The initial model should have a conductivity that permits the sensitivity of the latest decay times to reach the bottom of the model. If the initial conductivity is too high, convergence will be slower because the first iterations will not contain information about the conductivity at the deeper parts of the model.

The model covariance matrix

We shall adopt a model covariance matrix based on a von Karman covariance function. The general expression for these functions is

$$\Phi_{\nu,L}(z) = \sigma^2 \frac{2^{1-\nu}}{\Gamma(\nu)} \left(\frac{|z|}{L}\right)^{\nu} K_{\nu}\left(\frac{|z|}{L}\right) \tag{12}$$

where K_{ν} is the modified Bessel function of the second kind and order ν, Γ is the gamma function, L is the maximum correlation length accounted for and σ controls the amplitude. For $\nu \to 0$, the von Karman function effectively contains all correlation lengths

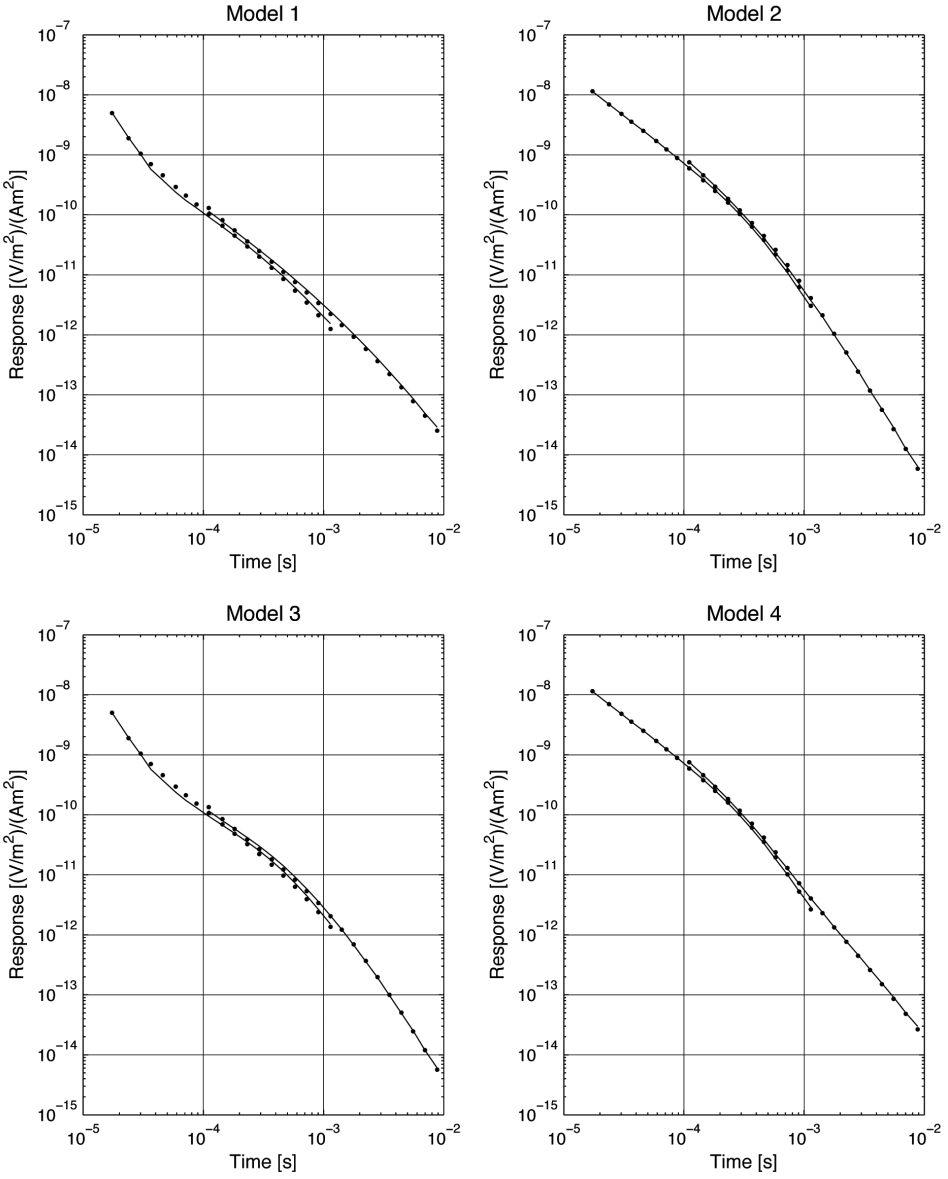

FIGURE 2
SkyTEM responses for the four test models. The two curves are for the low and high transmitter moment. Solid lines are conventional forward modelling; approximate forward responses are shown with dots. The radius of the dots corresponds to ≈8%.

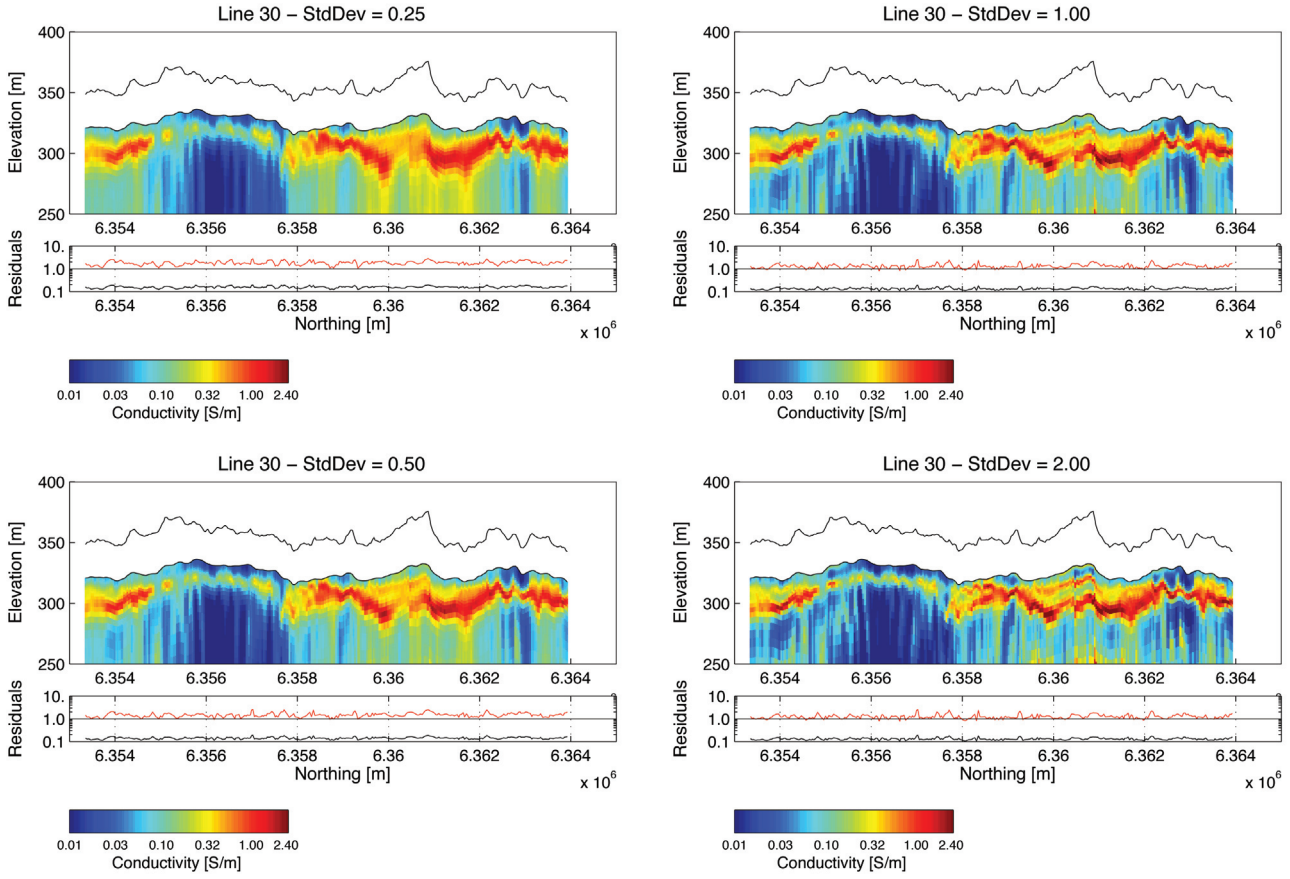

FIGURE 3

Model section of Line 30 for different values of the standard deviation of the model covariance matrix (σ_0 in equation (12)). The smaller the standard deviation, the tighter the smoothness constraint. A standard deviation of 1.00 strikes a compromise between inversion stability and resolution and is chosen for the whole survey.

due to the logarithmic singularity of K_0. This broadband behaviour ensures superior robustness in the inversion, i.e., model structure on all scales will be permitted if required by the data and it makes the regularization imposed by the model covariance matrix insensitive to the discretization (Serban and Jacobsen 2001).

A good approximation to the von Karman functions that allows rapid calculation and analytical integration over model elements can be achieved by stacking single-scale exponential covariance functions with different correlation lengths. Serban and Jacobsen (2001) showed this is possible if we choose

$$\Phi_{\nu,L_N} \approx \sigma_0^2 \sum_{n=0}^{N} C^{n\cdot\nu} \exp\left(-\frac{|z|}{C^n L_N \cdot 0.65}\right) \tag{13}$$

where L_N is the maximum correlation length represented, C is the factor ($C < 1$) between the correlation lengths, N is the number of stacked single-scale covariance functions and σ_0 is the standard deviation of the correlation. The factor 0.65 in the exponential denominator is an empirical factor that improves the fit to the von Karman function. The resulting stacked covariance function is essentially free of correlation scale. The lower and upper limits of the correlation lengths are a mathematical convenience and do not influence the correlation properties at the distance scales typically studied.

In this study we have used $\nu = 0.1$, $C = 0.1$, $L_N = 10\,000$ km and $N = 10$. This means that the covariance function will contain correlation lengths between 6,500 km and 6.5 mm, one per decade. This covers scales of geological variability between the radius of the Earth and pebbles; clearly sufficient for the resolution capability of airborne TEM data. Notice that the model covariance matrix only depends on the geometry of the multi-layer model and so it needs to be calculated and inverted only once.

The general expression for the elements of C_m for the single-scale correlation function with correlation length L, between the layers defined by the depth intervals of $[z_1, z_2]$ and $[z_3, z_4]$, is given by:

$$C_{i,j} = \frac{\sigma_0^2}{d_1 d_2} \int_{z_1}^{z_2} dz_0 \int_{z_3}^{z_4} \exp\left[-|z - z_0|/L\right] dz, d_1 = z_2 - z_1, d_2 = z_4 - z_3$$

$$= \frac{\sigma_0^2}{d_1 d_2} L^2 \left\{ e^{-(z_3 - z_2)/L} - e^{-(z_3 - z_1)/L} - e^{-(z_4 - z_2)/L} + e^{-(z_4 - z_1)/L} \right\} \tag{14}$$

For the autocorrelation of a layer in the depth interval $[z_1, z_2]$, the integration must be split into two intervals according to the sign of $(z-z_0)$

$$C_{i,i} = \frac{\sigma_0^2}{d^2}\int_{z_1}^{z_2} dz_0 \left\{ \int_{z_1}^{z_0} C_0 \exp\left[-(z_0 - z)/L\right] dz + \int_{z_0}^{z_2} C_0 \exp\left[-(z - z_0)/L\right] dz \right\}$$

$$= 2C_0 \frac{L}{d}\left\{1 - \frac{1-e^{-d/L}}{d/L}\right\}, d = z_2 - z_1 \qquad (15)$$

Choosing the regularization level of the multi-layer inversion

It is crucial for the inversion to choose the correlation standard deviation, σ_0, correctly in relation to the information content of the data. If σ_0 is too small, the model will not show all the structure that can be resolved by the data and if σ_0 is too large, the models will become erratic and the inversion will fit the data noise. The practical inversion is done on the logarithm of resistivities and the model covariance matrix thus relates to this parameter.

In Fig. 3, selected model sections for a range of standard deviations, σ_0, between 0.25–2.00 are shown for the approximate inversion. The smaller the standard deviation, the tighter the smoothness constraint and a pragmatic choice is made by inspection of the model sections. A standard deviation of 1.00 strikes a compromise between inversion stability and resolution and is chosen for the whole survey.

Choosing the regularization level of the lateral parameter correlation

Because of the local character of the data noise in space and time, individual inversion of the sounding data does not ensure lateral continuity of the model sections. However, based on the results of previous investigations in the Toolibin area we expect lateral changes in conductivity to be small and it is therefore reasonable to impose continuity by lateral correlation of the models. Techniques for lateral correlation of 1D earth models have been presented in the literature (e.g., Gyulai and Ormos 1999; Auken and Christiansen 2004). In this paper we use the lateral parameter correlation procedure of Christensen and Tølbøll (2009) for correlating models along the profiles (see Appendix A for a brief description). The fundamental characteristic of the lateral parameter correlation method is that it sepa-

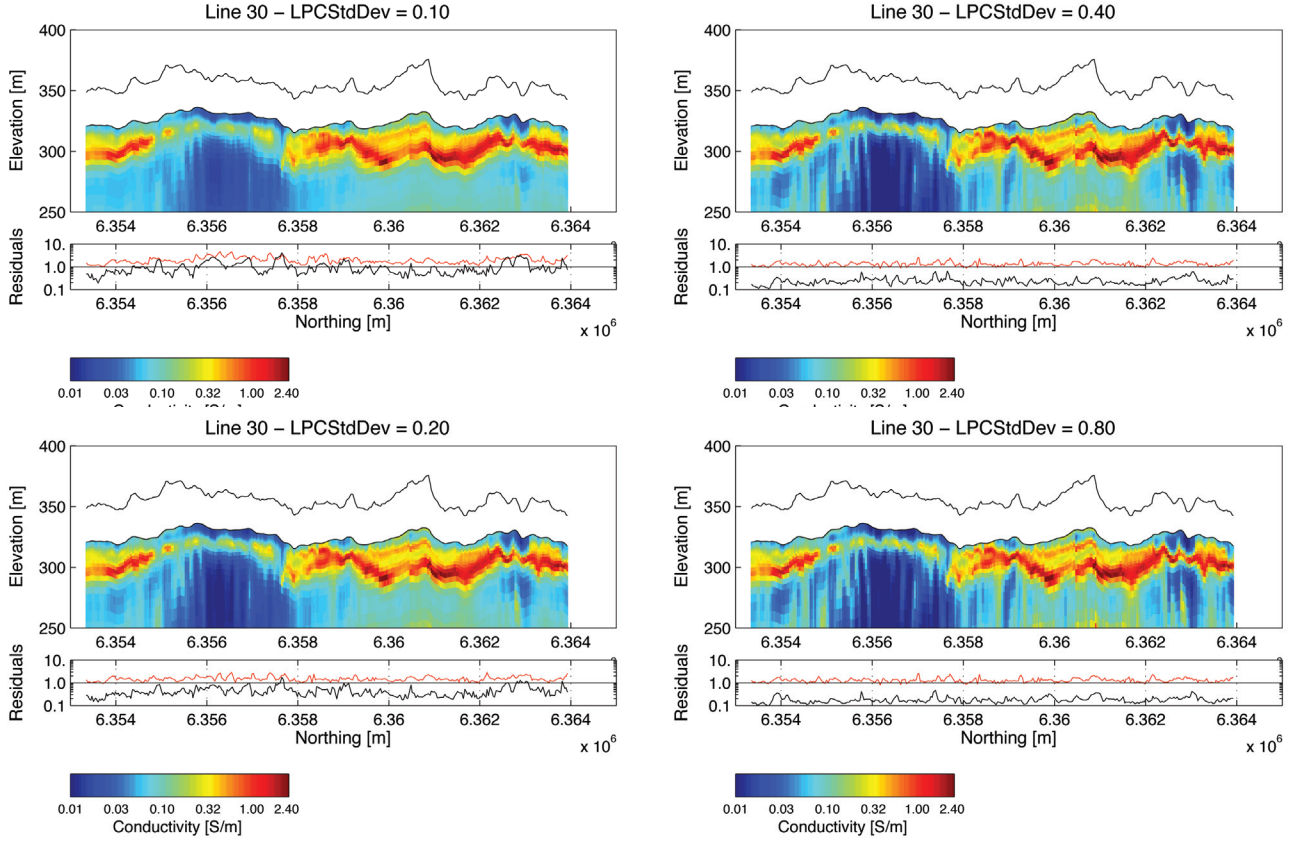

FIGURE 4

Model section of Line 30 for different values of the standard deviation of the model covariance matrix (σ_0 in equation (12)) in the lateral parameter correlation procedure. The smaller the standard deviation, the tighter the smoothness constraint. A standard deviation of 0.2 strikes a compromise between lateral smoothness and resolution and is chosen for the whole survey.

rates the inversion from the lateral correlation. This makes the method much faster than other methods of lateral correlation relying on a simultaneous inversion of a large number of soundings including lateral constraint in every iterative step.

After having obtained a model section consisting of individually inverted models, all with the same number of layers, the correlation is carried out on the model parameters, one at a time by solving an inversion problem involving a covariance matrix for smoothness. For multi-layer models, correlation is only done on layer conductivities or log(resistivities) because all layer boundaries are fixed. For large surveys, the inversion problem of the correlation can be segmented into overlapping regions to reduce computation time. As a consequence of the smoothing involved in the correlation process, the correlated models do not generally fit the data as well as the uncorrelated models. To remedy this, without giving up the smoothness of the correlated models, a subsequent constrained inversion of the data is performed with the correlated values as *a priori* model parameters. As shown in Christensen and Tølbøll (2009), the lateral parameter correlation method has the desired effect that well determined parameters have more influence on the correlated models than poorly determined parameters.

We have chosen to use the same broadband covariance matrix for the lateral correlation as for the vertical smoothness. Using the broadband covariance matrix is equivalent to an assumption that the variability of the geology is fractal and using the same for vertical and horizontal regularization means that we have no assumptions that the vertical and horizontal variability are different. As for the vertical smoothness, it is crucial to choose the correlation standard deviation, σ_0, correctly for the lateral parameter correlation procedure. In Fig. 4, selected model sections for a range of standard deviations, σ_0, between 0.1–0.8 are shown for the lateral correlation of log(resistivities). The smaller the standard deviation, the tighter the smoothness constraint and a pragmatic choice can be made by inspection of the model sections. A standard deviation of 0.2 strikes a compromise between lateral smoothness and resolution and is chosen for the whole survey.

FIELD EXAMPLE: THE TOOLIBIN LAKE SURVEY, AUSTRALIA

Geology of the survey area

Toolibin Lake is located approximately 250 km south-east of Perth, Western Australia (see Fig. 5). The groundwater and surface water hydrology of the lake have been extensively studied due to the significant dry land salinity problems that occur in the area (George 1998; George and Dogramaci 2000; Dogramaci *et al.* 2003; Reid *et al.* 2007). Groundwater investigations have included extensive shallow drilling, downhole induction logging and surface and airborne electromagnetics and airborne magnetic and radiometric surveys (Lane and Pracilio 2000; Dogramaci *et al.* 2003). Two previous airborne electromagnetic surveys have been flown over the lake using the SALTMAP and TEMPEST systems (Lane and Pracilio 2000; Street *et al.* 2002). This extensive geophysical and hydrogeological data set and its relative proximity to Perth make Lake Toolibin an excellent test range for new airborne geophysical methods.

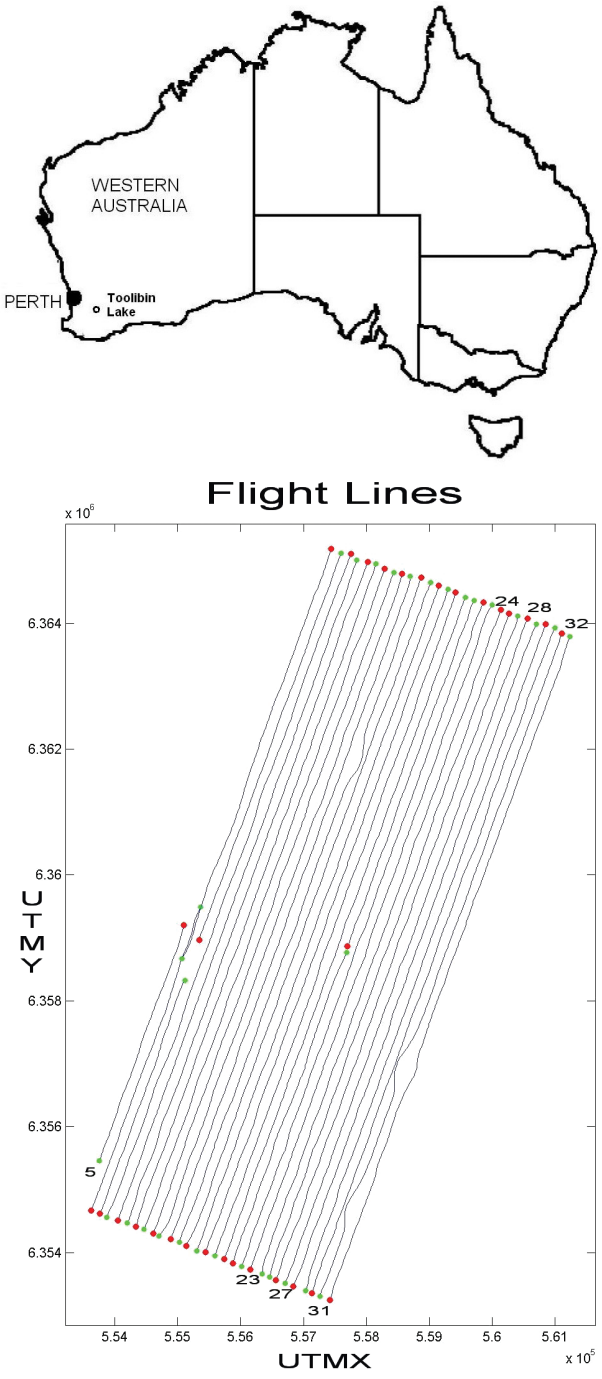

FIGURE 5
Location map of the Toolibin Lake area and flight lines of the 2006 survey.

The geology in the survey area comprises Quaternary and Tertiary alluvial sediments overlying weathered Archaean granite and granite gneiss of the Yilgarn Craton (Lane and Pracilio 2000). The granitic bedrock contains numerous Proterozoic

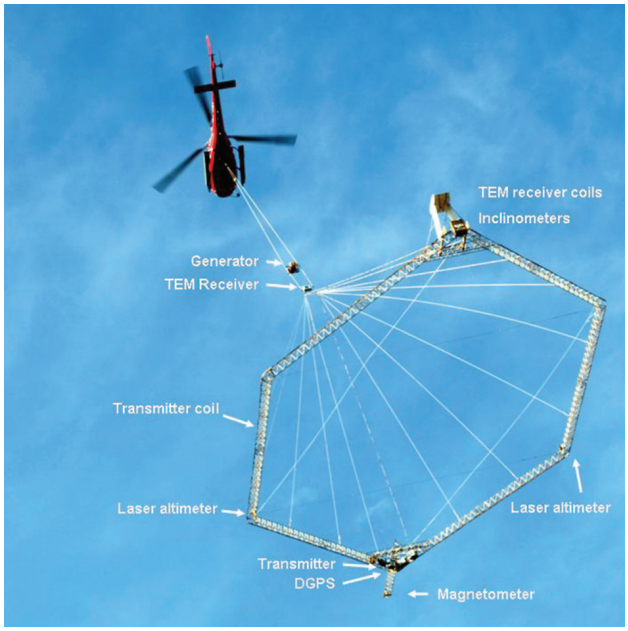

FIGURE 6
The SkyTEM system at a glance.

TABLE 1
The SkyTEM system parameters of the Toolibin Lake survey

Survey parameter	LM	HM
Tx area (m^2)	314	314
Tx turns	1	4
Tx current (A)	40	85
Tx moment (Am^2)	12,600	107,000
Nominal Tx height (m)	30	30
Repetition frequency (Hz)	222	25
Nominal ground speed (km/h)	80	80
First gate (μs)	11.2	47
Last gate (ms)	1.12	8.8
Number of gates	20	24
Stack size	160	64
Rx cutoff frequency (kHz)	450	450
Amplifier cutoff frequency (kHz)	225	225
Front gate (μs)	8	40

mafic dykes. Cover sequences overlying fresh bedrock are on average 25 m thick, with a maximum thickness of 60 m. Previous geophysical surveys at Toolibin Lake have shown the cover sequences to have conductivities of up to 700 mS/m as a result of very high groundwater salinity in the area (>50,000 mg/l in places). Fresh Archaean bedrock is generally of low conductivity, less than 0.01 S/m. Hydrogeological interpretation of over 100 drill holes and airborne geophysical data sets has revealed the presence of a deep and relatively transmissive palaeochannel system that extends about five kilometres north-east of the lake (Dogramaci *et al.* 2003). The palaeochannel sediments are composed of sands and clays up to 30 m thick and, beneath the lake itself, they are overlain by fine lacustrine clay up to eight metres thick. Inductive conductivity logs indicate that the palaeochannel sediments have slightly lower electrical conductivity than surrounding saprolitic clays.

The airborne TEM survey

The SkyTEM system (Fig. 6) is a helicopterborne TEM system (Sørensen and Auken 2004) originally designed and developed for hydrogeophysical and environmental investigations. The aim was to develop an airborne system that would give the same resolution as conventional ground-based TEM soundings.

The survey is fairly small comprising approximately 340 km on 32 lines (see Fig. 5). The investigated area coincides with the western part of a previous airborne EM survey flown in 1998 (Lane and Pracilio 2000). The survey was conducted using both a low and a high transmitter moment to ensure good near-surface resolution and good depth penetration, respectively. Measured data were horizontal in-line (x) and vertical (z) components, although only the z-component was used for quantitative interpretation. We are not yet quite satisfied with our approach to the more complicated processing scheme necessary for x-component data and considering that the x-component is also more prone to noise, we decided to exclude it from the inversion. The parameters of the survey for the low and high moments are seen in Table 1.

Data processing

Given the shallow depth of investigation required for the survey and the generally high signal strength due to the very high subsurface conductivities, SkyTEM data from Toolibin were subjected to a basic data processing of simple stacking. Laser altimeter data were processed using a local maximum filter to attempt to recover distance to the ground surface. Data from each of the altimeters were then corrected for the attitude (tilt) of the transmitter loop and to yield the height above ground of the transmitter loop centre. Final laser altitudes are averages of data from both altimeters. For a further discussion of these steps, please refer to Auken *et al.* (2009).

Inversion, data fit and data inconsistency

The 7,887 sets of combined low and high moment data were jointly inverted using the fast approximate inversion procedure outlined above with a standard deviation of the model covariance matrix used in controlling the vertical smoothness of the model of 1.00 and a standard deviation of the model covariance matrix used in the lateral parameter correlation procedure of 0.20. The initial individual inversions were carried out in around 0.25 s per sounding, the lateral parameter correlation procedure took around 4 min and the inversion after correlation was done in around 0.10 s per sounding.

In general, most of the soundings can be interpreted well with 1D models. Typical values of the normalized data residuals, equations (22)–(24), are of the order of 1–2, indicating that the noise model is reasonable. However, at certain locations, primarily where rapid changes in topography are present, inconsistency with the assumption of a 1D model will result in a poorer data fit.

Presentation of results: model sections

For each of the 32 survey lines, the models resulting from inversion of the individual sounding data are concatenated in model sections, plotted with Northing as a profile parameter. Each figure consists of two panels. The top plot shows the inverted models with topography where the conductivity of the individual layers are colour coded on a logarithmic scale according to the colour bar. The bird height is indicated as the black curve above the earth's surface in the model section. Below the model section is a plot of the residuals of the inversions: red indicates the data residual and black is the total residual. For reasons of space, we shall show model sections of two lines: Line 9 and Line 19 in Fig. 7.

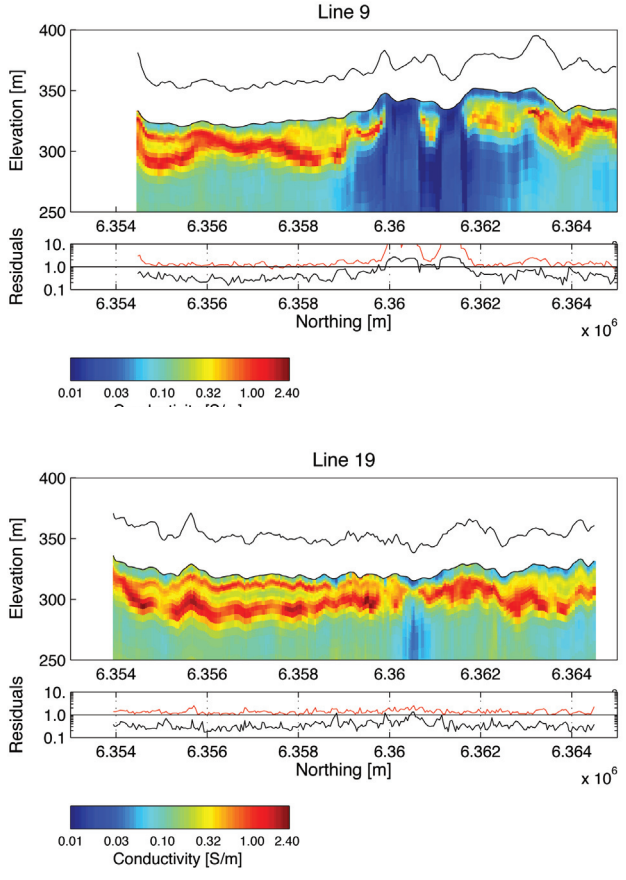

FIGURE 7

Model sections of concatenated 1D models from Line 9 and Line 19. The bird height is indicated as the black curve above the earth's surface in the model section (upper panel). Data residual (red) and total residual (black) are plotted in the lower panel.

Line 9 shows the fundamental units in the area: a 5–10 m thick cover of intermediate conductivity corresponding to alluvial sediments with a layer below of high conductivity corresponding to saprolitic clays: intensely weathered bedrock containing very saline groundwater. The bottom of the conductive layer is found at a depth of 40–60 m, where a less conductive unit is found that we interpret as the less conductive bedrock. This interpretation has been confirmed by drilling. Between N6,360,000 m and N6,362,000 m, a low conductivity area is found, indicating unweathered bedrock. This low conductivity zone corresponds to the area in the NW and SE part of the survey area indicated in the maps of mean conductivity in Fig. 8. Note also the good lateral resolution of the airborne data and the inversion procedure, specifically that the lateral parameter correlation procedure does not smear the high lateral contrast in conductivity at the edges of the outcrop.

In Line 19, which passes through the centre of the survey area, the conductive layer is split into an upper and a lower layer by a slightly less conductive layer at a depth of 20 m. This layer indicates the fine-grained lacustrine sediments beneath Lake Toolibin that appear in the mean conductivity maps in Fig. 8. Conductivity logging of boreholes drilled in the lake has shown these lacustrine sediments to be slightly less conductive than the underlying palaeochannel sands and gravels. It is presumed that the groundwater within these clays is less saline than those in the saprolites and palaeochanel sequence.

Presentation of results: contoured maps of mean conductivity

For the whole survey area, colour contoured maps of the mean conductivity in depth intervals have been produced. The mean conductivity in the elevation interval $[h_1; h_2]$ is defined as

$$< \sigma >= \frac{1}{h_2 - h_1} \int_{h_1}^{h_2} \sigma(z) dz \tag{16}$$

For a layered model with L layers, this expression can be found as a weighted sum of layer conductivities

$$< \sigma >= \frac{1}{h_2 - h_1} \sum_{i=1}^{L} w_i \cdot \sigma_i \tag{17}$$

where the weight factor w_i is the thickness of the part of the layer lying within the elevation interval $[h_1; h_2]$. Because the layer boundaries are fixed, the uncertainty of the mean conductivity depends only on the uncertainty of the layer conductivities and we have

$$\text{var} < \sigma >= \frac{1}{h_2 - h_1} \cdot \mathbf{w}^T \mathbf{C}^{\sigma}_{post} \mathbf{w} \tag{18}$$

where $\mathbf{C}^{\sigma}_{post}$ is the posterior covariance matrix of layer conductivities. However, the posterior covariance matrix $\boldsymbol{C}_{est}$ available after inversion refers to the logarithm of the resistivity, $\log \rho$ but the covariance of σ can be found from the covariance of $\log \rho$.

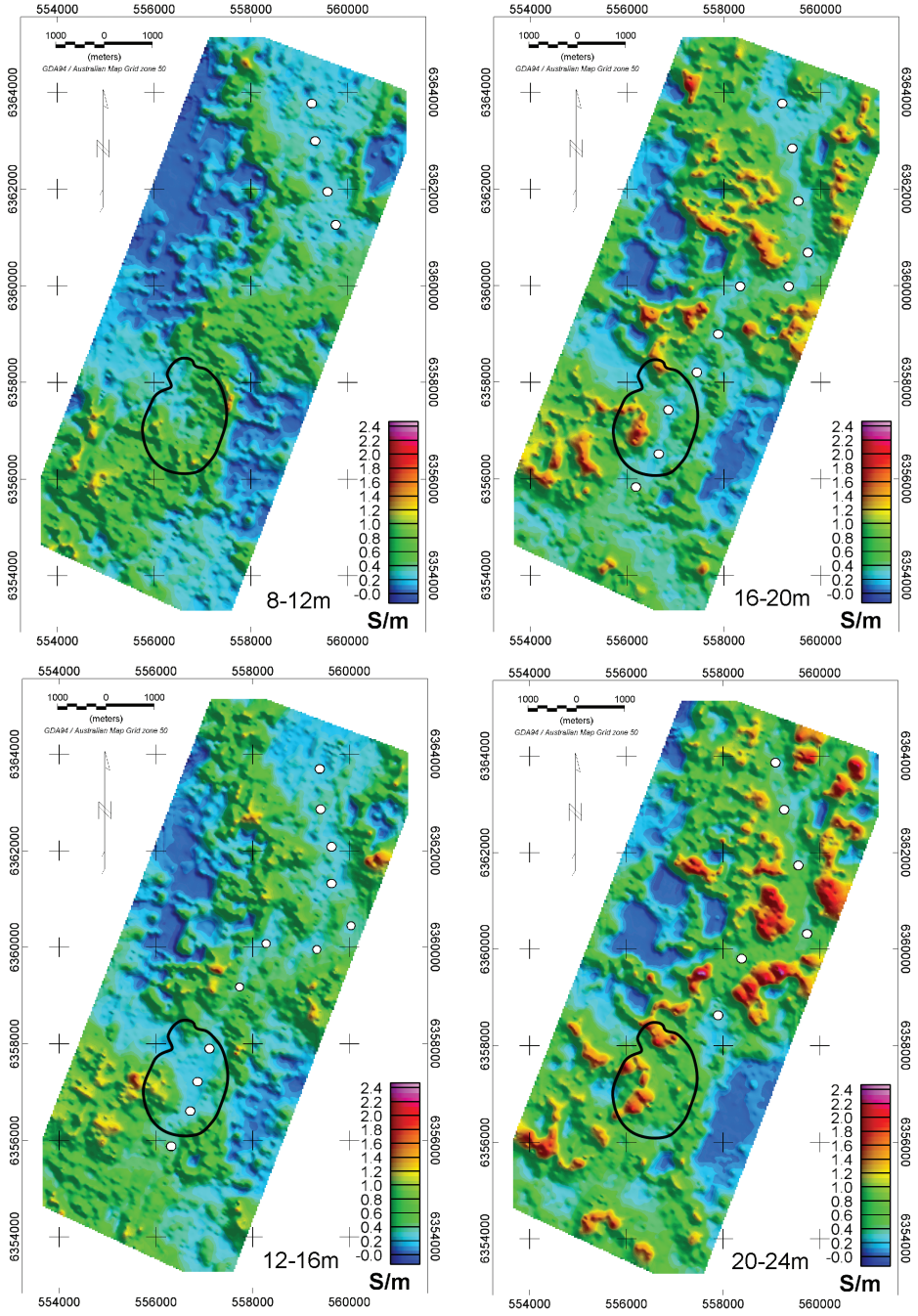

FIGURE 8
Colour contoured maps of mean conductivity in the depth intervals 8–12 m, 12–16 m, 16–20 m and 20–24 m. The outline of Tolibin Lake is seen as a black contour in the SW part of the area and the palaeochannel is marked with white dots.

Using that $\mathrm{var}[f(x)] \approx [f'(x)]^2\,\mathrm{var}(x)$ is correct to the first order, we find

$$\mathrm{cov}(\sigma_i,\sigma_j) = \sigma_i\sigma_j\,\mathrm{cov}(\log\sigma_i,\log\sigma_j) = \sigma_i\sigma_j\,\mathrm{cov}(-\log\rho_i,-\log\rho_j) \Rightarrow$$

$$\mathrm{cov}(\sigma_i,\sigma_j) = \sigma_i\sigma_j\,\mathrm{cov}(\log\rho_i,\log\rho_j) \qquad (19)$$

and thereby

$$\mathrm{var}(\sigma_i) = \sigma_i^2\,\mathrm{var}(\log\rho_i) \qquad (20)$$

For the mean of conductivities we therefore have

$$\mathrm{var} < \sigma >= \mathbf{w}^T\,\mathrm{diag}(\boldsymbol{\sigma})\mathbf{C}_{est}\,\mathrm{diag}(\boldsymbol{\sigma})\mathbf{w} \qquad (21)$$

where diag($\boldsymbol{\sigma}$) is the diagonal matrix containing the layer conductivities.

We have produced maps of the mean conductivity in depth intervals of 4 m thickness from 0–4 m to 40–44 m. For reasons of space, we shall show maps of only the four depth intervals 8–12 m, 12–16 m, 16–20 m and 20–24 m shown in Fig. 8. The

maps have been derived from the results of the approximate inversion including the lateral parameter correlation procedure. The survey identifies a relatively low conductivity palaeochannel trending from NE to SW through the survey area known to exist from previous surveys. The channel is seen in all four maps highlighted with white dots but most clearly in the 16–20 m interval, indicated by the light blue colours.

The relatively less conductive areas that are seen in the NW and SE parts of the survey area indicate where the less conductive bedrock lies closer to the surface. The highly conductive area in the southern part of the survey area in the 8–12 m map shows the conductive alluvium above Toolibin Lake itself. In the deeper mean conductivity maps it is seen that conductivity under the lake decreases as we enter the lacustrine sediments and palaeochannel sequence that are less conductive than the adjacent saprolitic clays.

Comparison with conventional inversion

In Fig. 9, model sections for Line 30 derived from fast approximate and conventional inversion are shown. In the comparison, the initial model, the regularization and all other inversion parameters were identical to the values chosen for the whole survey. It is seen that there is hardly any difference between the two sections.

To further compare the two inversion strategies, we have compared the mean of the normalized data residual, model residual and total residual of the conventional inversion and the forward responses of the models found in the approximate inversion on Line 30. These residuals are defined by

$$R_d = \sqrt{\frac{1}{N}\left(\mathbf{d}_{obs} - \mathbf{g}(\mathbf{m}_n)\right)^T \mathbf{C}_{obs}^{-1}\left(\mathbf{d}_{obs} - \mathbf{g}(\mathbf{m}_n)\right)} \tag{22}$$

$$R_m = \sqrt{\frac{1}{L}\left(\mathbf{m}_{prior} - \mathbf{m}_n\right)^T \mathbf{C}_{prior}^{-1}\left(\mathbf{m}_{prior} - \mathbf{m}_n\right)} \tag{23}$$

$$R_t = \sqrt{\frac{1}{N+L}\left(N \cdot R_d^2 + L \cdot R_m^2\right)} \tag{24}$$

and they measure the data misfit, the misfit between the prior model and the final model and a weighted sum of the two. The inversion minimizes the total residual.

In Table 2, the mean residuals are shown. The total residuals are almost the same, indicating that from an inversion point of view, the models of the approximate inversion are as good as the ones found in the conventional full inversion The model residuals are also very close, indicating that the model roughness is about the same for the two inversion approaches that is also indicated by the similarity of the model sections in Fig. 9. The data residual of the conventional forward response of the models found in the approximate inversion is 50% higher than that of the conventional inversion. We consider that to be a very good result, considering that the normalized residuals, equations (22)–(24), scale with the estimated noise level and that the uncertainty of the noise level estimate can be close to 50%.

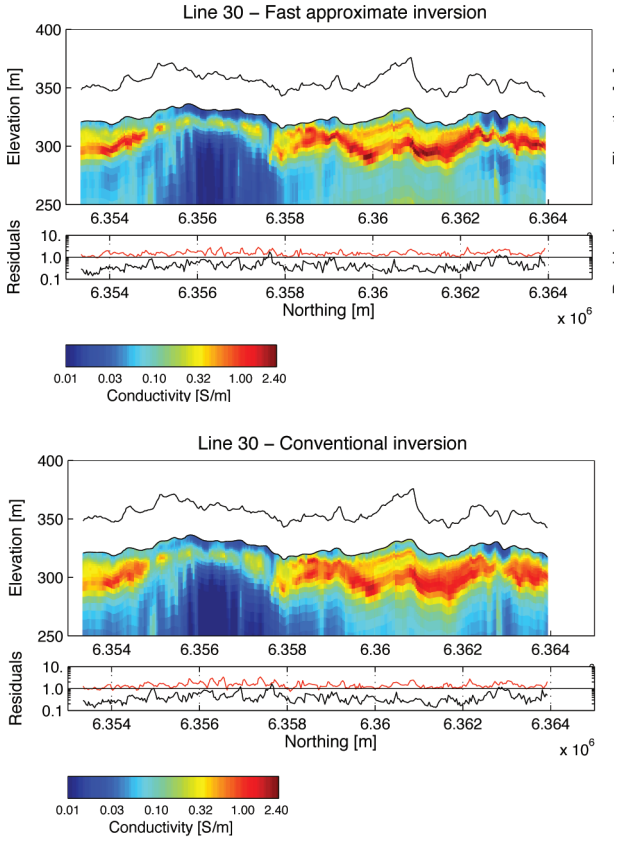

FIGURE 9

Model sections of Line 30 for the fast approximate inversion and for conventional inversion. The bird height is indicated as the black curve above the earth's surface in the model section (upper panel). Data residual (red) and total residual (black) are plotted in the lower panel.

CONCLUSIONS

We have presented a fast approximate inversion procedure for TEM data and applied it to the SkyTEM survey at Toolibin Lake, Australia.

The fast approximate inversion is very accurate as shown by comparisons between approximate and conventional forward responses for four simple models. A comparison of model sections from the fast and the conventional inversion shows very little difference; they are almost indistinguishable from one another.

Inversion of the Toolibin Lake survey has resolved the main features of the geology of the area: a top layer of 2–10 m of medium conductivity underlain by a very conductive layer with a thickness of 30–50 m. The high conductance of the layer is caused by the ubiquitous saltwater and – to a lesser extent – by the presence of clays. Below the conductive formation, the

TABLE 2
The residuals of the conventional inversion (left three) compared with the residuals between data and the conventional forward responses of the models obtained from fast approximate inversion (right three)

Residual type	Conventional inversion	Fast approximate inversion
Data	1.48	2.24
Model	0.51	0.55
Total	0.41	0.45

unweathered rock is found with a lower conductivity. In the SE and NW part of the survey area (see Fig. 8), the conductive middle layer is absent. Through the survey area, a SW-NE trending palaeochannel is found with conductivities slightly below that of the very conductive layer.

Considering the similarity between the results of the approximate and conventional inversion and that the approximate inversion is 50 times faster, it can be concluded that the approximate inversion offers a very attractive alternative to conventional inversion techniques. In cases where the emphasis is on structural information, no further inversion with conventional methods is necessary. In cases where the depth to layers boundaries between layers of sharp conductivity contrasts is needed, few-layer inversion must be carried out. The approximate inversion cannot be used in few-layer, parametric inversion but excellent starting models for the few-layer inversion can be inferred from the multi-layer models of the approximate inversion, thus ensuring stable convergence and considerably reducing computation time.

The fast approximate inversion makes it possible to invert data in the field as soon as they are downloaded from the instrument. A robust data processing followed by an approximate inversion with robust regularization enables the contractor and client to see the results of the measurements the same day the data are recorded. This enables daily changes to be made to the survey strategy and layout.

Fast approximate inversion will always be useful, no matter how fast computers will become because the number of measured data and the complication level of the processing and inversion also increase in proportion with the computer speed. The fast inversion offers itself as an integral part of any interpretation strategy, it is useful for quality control and it permits an adaptive measuring strategy.

REFERENCES

Auken E. 1995. 1D time domain electromagnetic interpretations over 2D and 3D structures. *Proceedings of the Symposium on the Application of Geophysics to Engineering and Environmental Problems*, Orlando, USA. EEGS, pp. 329–338.

Auken E. and Christiansen A.V. 2004. Layered and laterally constrained 2D inversion of resistivity data. *Geophysics* **69**, 752–761.

Auken E., Christiansen A.V., Jacobsen B.H., Foged N. and Sørensen K.I. 2005. Piecewise 1D laterally constrained inversion of resistivity data. *Geophysical Prospecting* **53**, 497–506.

Auken E., Christiansen A.V., Westergaard J.H., Kirkegaard C., Foged N., Viezzoli A. 2009. An integrated processing scheme for high-resolution airborne electromagnetic surveys, the SkyTEM system. *Exploration Geophysics* **40**, 184–192

Auken E., Pellerin L., Christensen N.B. and Sørensen K. 2006. A survey of current trends in near-surface electrical and electromagnetic methods. *Geophysics* **71**, G249–G260.

Brodie R. and Sambridge M. 2006. A holistic approach to inversion of frequency-domain airborne EM data. *Geophysics* **71**, G301–G312.

Buselli G., Barber C., Davis G.B. and Salama R.B. 1990. Detection of groundwater contamination near waste disposal sites with transient electromagnetic and electrical methods. In: *Geotechnical and Environmental Geophysics, Volume 2: Environmental and Groundwater* (ed. S.H. Ward), pp. 27–39. SEG.

Christensen N.B. 1990. Optimized fast Hankel transform filters. *Geophysical Prospecting* **38**, 545–568.

Christensen N.B. 2002. A generic 1-D imaging method for transient electromagnetic data. *Geophysics* **67**, 438–447.

Christensen N.B. and Sørensen K.I. 1998. Surface and borehole electric and electromagnetic methods for hydrogeophysical investigations. *European Journal of Environmental and Engineering Geophysics* **3**, 75–90.

Christensen N.B. and Tølbøll R.J. 2009. A lateral model parameter correlation procedure for one-dimensional inverse modelling. *Geophysical Prospecting* **57**, 919–929. doi:10.1111/j.1365-2478.2008.00756.x

Dogramaci S., George R., Mauger G. and Ruprecht J. 2003. Water balance and salinity trend, Toolibin catchment, Western Australia. http://www.naturebase.net/pdf/projects/salinity/toolibin/water_bal_salinity_trend.pdf.

Eaton P.A. and Hohmann G.W. 1989. A rapid inversion technique for transient electromagnetic soundings. *Physics of the Earth and Planetary Interiors* **53**, 384–404.

Fittermann D.V. and Stewart M.T. 1986. Transient electromagnetic sounding for groundwater. *Geophysics* **51**, 995–1005.

George R. 1998. *Evaluation of Airborne Geophysics for Catchment Management, Toolibin, Western Australia*. National Airborne Geophysics Project.

George R. and Dogramaci S. 2000. Toolibin - A life and death struggle for the last freshwater Wheatbelt lake. *3rd International Hydrology and Water Resources Symposium of the Institution of Engineers Australia*, 20–23 November 2000, Perth, Australia, pp. 733–738.

Goldman M., Tabarovsky L. and Rabinovich M. 1994. On the influence of 3-D structures in the interpretation of transient electromagnetic sounding data. *Geophysics* **59**, 889–901.

Gyulai A. and Ormos T. 1999. A new procedure for the interpretation of VES data: 1.5-D simultaneous inversion method. *Journal of Applied Geophysics* **64**, 1–17.

Hoekstra P. and Blohm M.W. 1990. Case histories of time-domain electromagnetic soundings in environmental geophysics. In: *Geotechnical and Environmental Geophysics, Volume 2: Environmental and Groundwater* (ed. S.H. Ward), pp. 1–16. SEG.

Hördt A. and Scholl C. 2004. The effect of local distortions on time-domain electromagnetic measurements. *Geophysics* **68**, 87–96.

Inman Jr J.R., Ryu J. and Ward S.H. 1975. Resistivity inversion. *Geophysics* **38**, 1088–1108.

Lane R. and Pracilio G. 2000. Visualisation of subsurface conductivity derived from airborne EM. *Proceedings of the SAGEEP 2000*, pp. 101–110.

Macnae J. 1997. Developments in broadband airborne electromagnetics in the past decade. *Proceedings of the 5th Decennial International Conference on Mineral Exploration,* pp. 387–398.

Macnae J., King A., Stolz E., Osmakoff A. and Blaha A. 1998. Fast AEM data processing and inversion. *Exploration Geophysics* **29**, 163–169.

Macnae J.C. and Lamontagne Y. 1987. Imaging quasi-layered conductive structures by simple processing of transient electromagnetic data. *Geophysics* **52**, 545–554.
Macnae J.C., Smith R., Polzer B.D, Lamontagne Y. and Klinkert P.S. 1991. Conductivity-depth imaging of airborne electromagnetic step-response data. *Geophysics* **56**, 102–114.
Menke W. 1989. *Geophysical Data Analysis: Discrete Inverse Theory*. Academic Press.
Nekut A.G. 1987. Direct inversion of time-domain electromagnetic data. *Geophysics* **52**, 1431–1435.
Newman G.A., Anderson W.L. and Hohmann G.W. 1987. Interpretation of transient electromagnetic soundings over three-dimensional structures for the central-loop configuration. *Geophysical Journal of the Royal Astronomical Society* **89**, 889–914.
Reid J., Munday T. and Fitzpatrick A. 2007. High-resolution airborne electromagnetic surveying for dryland salinity management: The Toolibin Lake SkyTEM case study. ASEG meeting 2007, Perth, Western Australia, Expanded Abstracts.
Sattel D. 2005. Inverting airborne electromagnetic (AEM) data with Zohdy's method. *Geophysics* **70**, G77–G85.
Sattel D. 2006. A brief discussion of helicopter time-domain EM systems. AESC2006, Melbourne, Australia, Expanded Abstracts.
Serban D.Z. and Jacobsen B.H. 2001. The use of broadband prior covariance for inverse palaeoclimate estimation. *Geophysical Journal International* **147**, 29–40.
Sørensen K.I. and Auken E. 2004. SkyTEM - A new high-resolution helicopter transient electromagnetic system. *Exploration Geophysics* **35**, 191–199.
Spies B. and Woodgate P. 2005. *Salinity Mapping Methods in the Australian Context*. Prepared for the Natural Resource Management Ministerial Council, Land and Water Australia, National Dryland Salinity Programme, Department of Environment and Heritage and the Department of Agriculture, Fisheries and Forestry. ISBN: 0642551286.
Stolz E. and Macnae J. 1997. Fast approximate inversion of TEM data. *Exploration Geophysics* **28**, 317–322.
Stolz E.M. and Macnae J.C. 1998. Evaluating EM waveforms by singular-value decomposition of exponential basis functions. *Geophysics* **63**, 64–74. (Errata in *Geophysics* **64**, 310).
Street G.J., Pracilio G. and Anderson-Mayes A. 2002. Interpretation of geophysical data for salt hazard identification and catchment management in Southwest Western Australia. *Exploration Geophysics* **33**, 65–72.
Ward S.H. and Hohmann G.W. 1987. Electromagnetic theory for geophysical applications. In: *Electromagnetic Methods in Applied Geophysics* (ed. M.N. Nabighian), pp. 131–311. SEG.

APPENDIX A

The lateral correlation procedure

Techniques for lateral correlation of 1D earth models have been presented in the literature by e.g., Gyulai and Ormos (1999) and Auken and Christiansen (2004). In this appendix we give a brief description of the lateral parameter correlation procedure of Christensen and Tølbøll (2009).

Having obtained a model section consisting of individually inverted models, all with the same number of layers, the correlation is carried out on the model parameters, one at a time. Correlation can be done on layer conductivities or log(resistivities), layer thicknesses and depths to or elevation of layer boundaries but, evidently, for multi-layer models only on conductivities or log(resistivities). The values of the selected parameter for all models are collected in the parameter vector $\boldsymbol{p}$. The correlation is formulated as a constrained inversion problem where $\boldsymbol{p}$ plays the role of the data vector and the model vector that we wish to find, $\boldsymbol{p}_{cor}$, is a smoother version of $\boldsymbol{p}$. The forward mapping between $\boldsymbol{p}$ and $\boldsymbol{p}_{cor}$ is given by

$$\mathbf{p} = \mathbf{I}\mathbf{p}_{cor} + \mathbf{e} \tag{A1}$$

where $\boldsymbol{I}$ is the identity matrix and $\mathbf{e}$ is the observational error. The smoothing is realized by inverting the above relationship incorporating a model covariance matrix $\boldsymbol{C}_m$. In the present study, we have used the broadband covariance matrix defined in equation (12) that was also used for the vertical regularization of the multi-layer models. With no *a priori* constraints on $\boldsymbol{p}_{cor}$ the inversion of equation (A1) gives

$$\mathbf{p}_{cor} = \left(\mathbf{I}^T\mathbf{C}_p^{-1}\mathbf{I} + \mathbf{C}_m^{-1}\right)^{-1}\mathbf{I}^T\mathbf{C}_p^{-1}\mathbf{p} = \left(\mathbf{C}_p^{-1} + \mathbf{C}_m^{-1}\right)^{-1}\mathbf{C}_p^{-1}\mathbf{p} \tag{A2}$$

$\boldsymbol{C}_p$ is a diagonal error covariance matrix of the uncorrelated parameters. Its elements are the variances of the parameters of the uncorrelated models.

The standard deviations of the correlated model parameters are finally estimated as the square root of the diagonal elements of the posterior covariance matrix $\boldsymbol{C}_{est}$ given as

$$\mathbf{C}_{est} = \left(\mathbf{C}_p^{-1} + \mathbf{C}_m^{-1}\right)^{-1} \tag{A3}$$

As mentioned, the inversion problem is solved for each parameter separately. For large data sets the inversion problem may become quite large and the solution thereby time-consuming. This is, however, easily remedied by dividing the data set into smaller, overlapping segments of appropriate lengths.

As a consequence of the smoothing involved in the correlation process, the correlated models do not generally fit the data as well as the uncorrelated models. To remedy this, without giving up the smoothness of the correlated models, a subsequent constrained inversion of the data is performed with the correlated values $\boldsymbol{p}_{cor}$ as *a priori* model parameters – the $\boldsymbol{m}_{prior}$ vector of equations (10) and (11) – and a covariance matrix of the prior values – the $\boldsymbol{C}_{prior}$ matrix of equations (10) and (11) – defined by the variances of $\boldsymbol{p}_{cor}$.

The above method of lateral correlation is thus a three-step process: 1) individual inversion of the soundings, 2) lateral correlation of the model parameters, one at a time, formulated as a constrained inversion with a model covariance matrix and 3) repeated data inversion to ensure good data fit with the correlated parameters as *a priori* information. The lateral parameter correlation method does not depend on data lying on a straight line or being equidistant as the model covariance matrix is based on the lateral distance between the models. It is also possible to correlate models obtained by inversion of different data types and to incorporate information from other sources, e.g., drill hole information.

Because correlation is done on one parameter at a time, for multi-layer models it will follow the shape of the terrain. If the aim is to invoke horizontal smoothness, this is not really desirable but the situation can be alleviated by choosing the scaled distance between sounding positions as

$$r_{i,j} = \sqrt{(x_i - x_j)^2 + (y_i - y_j)^2 + \alpha^2 \cdot (z_i - z_j)^2} \quad \text{(A4)}$$

The higher the value of α, the more the correlation is subdued between points not at the same horizontal level.